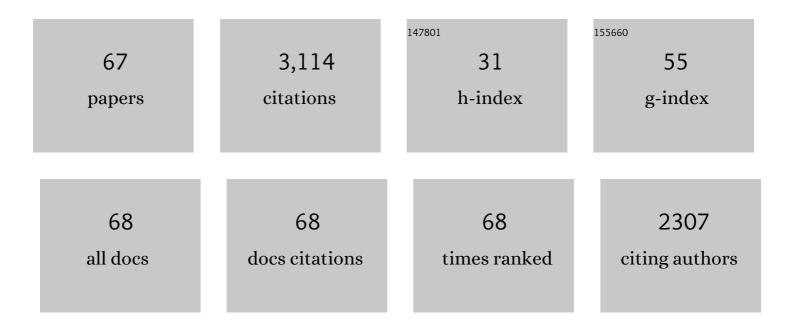
Yang Shen

List of Publications by Year in descending order

Source: https://exaly.com/author-pdf/4399732/publications.pdf Version: 2024-02-01



VANC SHEN

#	Article	IF	CITATIONS
1	Geochemical constraints on initial and final depths of melting beneath mid-ocean ridges. Journal of Geophysical Research, 1995, 100, 2211-2237.	3.3	216
2	Seismic evidence for a lower-mantle origin of the Iceland plume. Nature, 1998, 395, 62-65.	27.8	214
3	Phase Velocities of Rayleigh Waves in the MELT Experiment on the East Pacific Rise. Science, 1998, 280, 1235-1238.	12.6	197
4	Mantle flow, melting, and dehydration of the Iceland mantle plume. Earth and Planetary Science Letters, 1999, 165, 81-96.	4.4	172
5	Unsplit complex frequency-shifted PML implementation using auxiliary differential equations for seismic wave modeling. Geophysics, 2010, 75, T141-T154.	2.6	168
6	A complex Tibetan upper mantle: A fragmented Indian slab and no south-verging subduction of Eurasian lithosphere. Earth and Planetary Science Letters, 2012, 333-334, 101-111.	4.4	117
7	Upper mantle structure beneath the Azores hotspot from finite-frequency seismic tomography. Earth and Planetary Science Letters, 2006, 250, 11-26.	4.4	116
8	Imaging seismic velocity structure beneath the Iceland hot spot: A finite frequency approach. Journal of Geophysical Research, 2004, 109, .	3.3	109
9	The distribution of the midâ€ŧo″ower crustal lowâ€velocity zone beneath the northeastern Tibetan Plateau revealed from ambient noise tomography. Journal of Geophysical Research: Solid Earth, 2014, 119, 1954-1970.	3.4	97
10	Seismic evidence for a tilted mantle plume and north–south mantle flow beneath Iceland. Earth and Planetary Science Letters, 2002, 197, 261-272.	4.4	76
11	Upper mantle structure of the Cascades from full-wave ambient noise tomography: Evidence for 3D mantle upwelling in the back-arc. Earth and Planetary Science Letters, 2014, 390, 222-233.	4.4	73
12	Finite frequency tomography in southeastern Tibet: Evidence for the causal relationship between mantle lithosphere delamination and the north–south trending rifts. Journal of Geophysical Research, 2008, 113, .	3.3	71
13	The effects of temperature―and pressureâ€dependent viscosity on threeâ€dimensional passive flow of the mantle beneath a ridgeâ€transform System. Journal of Geophysical Research, 1992, 97, 19717-19728.	3.3	70
14	Seismic evidence for a Moho offset and south-directed thrust at the easternmost Qaidam–Kunlun boundary in the Northeast Tibetan plateau. Earth and Planetary Science Letters, 2009, 288, 329-334.	4.4	67
15	Upper mantle structures beneath the Carpathian–Pannonian region: Implications for the geodynamics of continental collision. Earth and Planetary Science Letters, 2012, 349-350, 139-152.	4.4	66
16	Three-dimensional anisotropic seismic wave modelling in spherical coordinates by a collocated-grid finite-difference method. Geophysical Journal International, 2012, 188, 1359-1381.	2.4	66
17	An Improved Method to Extract Very-Broadband Empirical Green's Functions from Ambient Seismic Noise. Bulletin of the Seismological Society of America, 2012, 102, 1872-1877.	2.3	65
18	Two forms of volcanism: Implications for mantle flow and offâ€axis crustal production on the west flank of the southern East Pacific Rise. Journal of Geophysical Research, 1993, 98, 17875-17889.	3.3	62

YANG SHEN

#	Article	IF	CITATIONS
19	Mantle Discontinuity Structure Beneath the Southern East Pacific Rise from P-to-S Converted Phases. Science, 1998, 280, 1232-1235.	12.6	61
20	Abundant seamounts of the Rano Rahi seamount field near the Southern East Pacific Rise, 15ïį½ S to 19ïį½ S. Marine Geophysical Researches, 1996, 18, 13-52.	1.2	55
21	Upper Mantle Earth Structure in Africa From Fullâ€Wave Ambient Noise Tomography. Geochemistry, Geophysics, Geosystems, 2019, 20, 120-147.	2.5	55
22	Seismic evidence for accumulated oceanic crust above the 660-km discontinuity beneath southern Africa. Geophysical Research Letters, 2003, 30, .	4.0	44
23	Hot mantle transition zone beneath Iceland and the adjacent Mid-Atlantic Ridge inferred from P-to-S conversions at the 410- and 660-km discontinuities. Geophysical Research Letters, 1996, 23, 3527-3530.	4.0	43
24	High resolution regional seismic attenuation tomography in eastern Tibetan Plateau and adjacent regions. Geophysical Research Letters, 2011, 38, n/a-n/a.	4.0	43
25	Seismic evidence for significant melt beneath the Long Valley Caldera, California, USA. Geology, 2018, 46, 799-802.	4.4	42
26	Numerical simulation of strong ground motion for the M s8.0 Wenchuan earthquake of 12 May 2008. Science in China Series D: Earth Sciences, 2008, 51, 1673-1682.	0.9	41
27	Trade-off in production between adjacent seamount chains near the East Pacific Rise. Nature, 1995, 373, 140-143.	27.8	39
28	Thermal, hydrous, and mechanical states of the mantle transition zone beneath southern Africa. Earth and Planetary Science Letters, 2004, 217, 367-378.	4.4	39
29	Mesoscale convective system surface pressure anomalies responsible for meteotsunamis along the U.S. East Coast on June 13th, 2013. Scientific Reports, 2014, 4, 7143.	3.3	39
30	Wave speed structure of the eastern North American margin. Earth and Planetary Science Letters, 2017, 459, 394-405.	4.4	37
31	Seismological evidence for a mid-mantle discontinuity beneath Hawaii and Iceland. Earth and Planetary Science Letters, 2003, 214, 143-151.	4.4	36
32	Shear wave structure in the northeastern Tibetan Plateau from Rayleigh wave tomography. Journal of Geophysical Research: Solid Earth, 2013, 118, 4170-4183.	3.4	34
33	Seismic wave speed structure of the Ontong Java Plateau. Earth and Planetary Science Letters, 2015, 420, 140-150.	4.4	31
34	Investigation of microearthquake activity following an intraplate teleseismic swarm on the west flank of the Southern East Pacific Rise. Journal of Geophysical Research, 1997, 102, 459-475.	3.3	30
35	Finite-frequency sensitivity kernels for head waves. Geophysical Journal International, 2007, 171, 847-856.	2.4	29
36	Crustal and upper mantle structure beneath the northeastern Tibetan Plateau from joint analysis of receiver functions and Rayleigh wave dispersions. Geophysical Journal International, 2016, 204, 583-590.	2.4	29

YANG SHEN

#	Article	IF	CITATIONS
37	Crustal and mantle velocity models of southern Tibet from finite frequency tomography. Journal of Geophysical Research, 2011, 116, .	3.3	28
38	Imaging Rayleigh wave attenuation with USArray. Geophysical Journal International, 2016, 206, 241-259.	2.4	27
39	Seismic evidence for a possible deep crustal hot zone beneath Southwest Washington. Scientific Reports, 2017, 7, 7400.	3.3	25
40	Cross-dependence of finite-frequency compressional waveforms to shear seismic wave speeds. Geophysical Journal International, 2008, 174, 941-948.	2.4	21
41	Validation of Shear-Wave Velocity Models of the Pacific Northwest. Bulletin of the Seismological Society of America, 2012, 102, 2611-2621.	2.3	20
42	A Preliminary Fullâ€Wave Ambientâ€Noise Tomography Model Spanning from the Juan de Fuca and Gorda Spreading Centers to the Cascadia Volcanic Arc. Seismological Research Letters, 2015, 86, 1253-1260.	1.9	20
43	Frequency-Dependent Crustal Correction for Finite-Frequency Seismic Tomography. Bulletin of the Seismological Society of America, 2006, 96, 2441-2448.	2.3	18
44	Array-Based Convolutional Neural Networks for Automatic Detection and 4D Localization of Earthquakes in Hawaiâ€~i. Seismological Research Letters, 2021, 92, 2961-2971.	1.9	17
45	Coupled seismic slip on adjacent oceanic transform faults. Geophysical Research Letters, 2003, 30, .	4.0	16
46	Threeâ€Dimensional Passiveâ€Source Reverseâ€Time Migration of Converted Waves: The Method. Journal of Geophysical Research: Solid Earth, 2018, 123, 1419-1434.	3.4	14
47	Azimuthal anisotropy of <i>Lg</i> attenuation in eastern Tibetan Plateau. Journal of Geophysical Research, 2012, 117, .	3.3	13
48	Validation of recent shear wave velocity models in the United States with fullâ€wave simulation. Journal of Geophysical Research: Solid Earth, 2015, 120, 344-358.	3.4	13
49	Crustal Velocity Structure of the Northeastern Tibetan Plateau from Ambient Noise Surface-Wave Tomography and Its Tectonic Implications. Bulletin of the Seismological Society of America, 2014, 104, 1045-1055.	2.3	12
50	P-wave velocity structure of the crust and uppermost mantle beneath Iceland from local earthquake tomography. Earth and Planetary Science Letters, 2005, 235, 597-609.	4.4	11
51	Growth of the northeastern margin of the Tibetan Plateau by squeezing up of the crust at the boundaries. Scientific Reports, 2017, 7, 10591.	3.3	11
52	A Cost-Effective Geodetic Strainmeter Based on Dual Coaxial Cable Bragg Gratings. Sensors, 2017, 17, 842.	3.8	11
53	Seismicity at the southern East Pacific Rise from recordings of an ocean bottom seismometer array. Journal of Geophysical Research, 2002, 107, EPM 9-1-EPM 9-11.	3.3	10
54	Detecting Slow Slip Events From Seafloor Pressure Data Using Machine Learning. Geophysical Research Letters, 2020, 47, e2020GL087579.	4.0	10

YANG SHEN

#	Article	IF	CITATIONS
55	Fullâ€Waveform Sensitivity Kernels of Componentâ€Differential Traveltimes and ZH Amplitude Ratios for Velocity and Density Tomography. Journal of Geophysical Research: Solid Earth, 2018, 123, 4829-4840.	3.4	9
56	Modeling Threeâ€Dimensional Wave Propagation in Anelastic Models With Surface Topography by the Optimal Strong Stability Preserving Rungeâ€Kutta Method. Journal of Geophysical Research: Solid Earth, 2019, 124, 890-907.	3.4	9
57	Earlyâ€Stage Lithospheric Foundering Beneath the Eastern Tibetan Plateau Revealed by Fullâ€Wave <i>P</i> _n Tomography. Geophysical Research Letters, 2020, 47, e2019GL086469.	4.0	9
58	Accurate source location from waves scattered by surface topography. Journal of Geophysical Research: Solid Earth, 2016, 121, 4538-4552.	3.4	6
59	An OBS Array to Investigate Offshore Seismicity during the 2018ÂKÄ«lauea Eruption. Seismological Research Letters, 2021, 92, 603-612.	1.9	6
60	Assessing waveform predictions of recent threeâ€dimensional velocity models of the Tibetan Plateau. Journal of Geophysical Research: Solid Earth, 2016, 121, 2521-2538.	3.4	5
61	Location and moment tensor inversion of small earthquakes using 3D Green's functions in models with rugged topography: application to the Longmenshan fault zone. Earthquake Science, 2016, 29, 139-151.	0.9	5
62	Initial rupture processes of the 2008 Mw7.9 Wenchuan, China earthquake: From near-source seismic records. Journal of Asian Earth Sciences, 2019, 173, 397-403.	2.3	5
63	Component-Dependent Frechet Sensitivity Kernels and Utility of Three-Component Seismic Records. Bulletin of the Seismological Society of America, 2008, 98, 2517-2525.	2.3	4
64	Effects of seasonal changes in ambient noise sources on monitoring temporal variations in crustal properties. Journal of Seismology, 2015, 19, 781-790.	1.3	4
65	Compositional Variation in the Crust of Peninsular Ranges and Surrounding Regions, Southern California, Revealed by Fullâ€Wave Seismic and Gravity Joint Inversion. Journal of Geophysical Research: Solid Earth, 2021, 126, .	3.4	4
66	An Improved Earthquake Catalog During the 2018 KıÌ,,lauea Eruption From Combined Onshore and Offshore Seismic Arrays. Earth and Space Science, 2022, 9, .	2.6	2
67	Locating Shallow Seismic Sources With Waves Scattered by Surface Topography: Validation of the Method at the Nevada Test Site. Journal of Geophysical Research: Solid Earth, 2019, 124, 7040-7051.	3.4	0